

THE NATURE OF COMPOSITE SEYFERT/STAR-FORMING GALAXIES REVEALED BY X-RAY OBSERVATIONS

FRANCESCA PANESSA^{1,2}, ANNA WOLTER³, SILVIA PELLEGRINI⁴, ANTONELLA FRUSCIONE², LOREDANA BASSANI⁵, ROBERTO DELLA CECA³, GIORGIO G.C. PALUMBO⁴, GINEVRA TRINCHIERI³

Draft version

ABSTRACT

This paper presents new *Chandra* and *BeppoSAX* observations aimed at investigating the optical/X-ray mismatch in the enigmatic class of the Composite galaxies, discovered by a cross-correlation of IRAS and ROSAT all sky survey catalogues. These galaxies have been classified as star-forming objects on the basis of their optical spectra, while the detection of weak broad wings in the H α emission in a few of them and their high X-ray luminosity in the ROSAT band indicated the presence of an active nucleus. The analysis of *Chandra* observations for 4 Composites has revealed nuclear point-like sources, with a typical AGN spectrum ($\Gamma \sim 1.7-1.9$) and little intrinsic absorption. A strong flux variability has been observed on different time scales, in particular most of the sources were brighter at the ROSAT epoch. Although of relative low luminosity for the AGN class ($L_{2-10keV} \sim 3-60 \times 10^{41}$ erg/s), the active nucleus is nevertheless dominant in the X-ray domain. At other wavelengths it appears to be overwhelmed by the starburst and/or host galaxy light, yielding the Composite classification for these objects.

Subject headings: x-ray: galaxies; galaxies: active, galaxies: starburst, galaxies: peculiar

1. INTRODUCTION

Evidence for a link between intense star formation and nuclear activity has grown steadily in recent years (e.g. Veilleux, 2001, Gonzales Delgado et al. 2001, and references therein). On one hand, the presence of circumnuclear starbursts in many local AGNs (e.g., Levenson et al. 2004, Levenson et al. 2001) suggests a connection not yet fully understood. The presence of a starburst has been invoked for instance to produce absorption in low luminosity AGNs (Fabian et al. 1998, Ohsuga & Umemura, 2001). On the other hand, the ubiquity of supermassive black holes in the nuclei of normal galaxies (Kormendy et al. 2002) and the proportionality between the black hole and the spheroidal masses (Ferrarese & Merrit 2000) evidence a direct link between the formation of ellipticals and spiral bulges and the growth of central black holes. Therefore, the interplay between accretion on supermassive black holes and galaxy formation and evolution has become a fundamental ingredient for theoretical models in this field (e.g., Springel et al. 2005, Sazonov et al. 2005, Nipoti et al. 2003). This implies that our view on the star formation history of the universe, as deduced by galaxy luminosity functions (see Springel et al. 2005), as well as on the chemical enrichment and feedback processes in the early universe, might change in a way that we cannot foresee at this moment. Understanding the connection between starburst and AGN in the local universe is therefore of crucial importance.

A spectroscopic optical survey of bright IRAS and X-

ray selected sources from the ROSAT All Sky Survey revealed a small enigmatic class of low redshift galaxies with optical spectra dominated by the features of H II galaxies but presenting very subtle Seyfert signatures as well. These objects had X-ray luminosities typical of broad line AGNs, ranging from 1.5×10^{42} erg/s to 5×10^{43} erg/s in the ROSAT band (Moran et al. 1996, hereafter M96). They were named Composite after their Composite optical spectra. The diagnostic emission line ratio diagrams (Veilleux & Osterbrock 1987) classify them either on the boundary between Seyfert and HII regions or as pure star-forming galaxies. Most of these galaxies show quite narrow emission lines (FWHM < 300 km/s) as HII galaxies normally do. Yet, some of them present [O III] $\lambda\lambda 4959, 5007$ lines significantly broader than all other narrow lines in the spectrum and weak and elusive broad H α wings. A possible scenario to explain the optical and X-ray mismatch proposed by M96 invokes absorption as responsible for the obscuration of the optical features. M96 also suggested that it is not likely that the starburst could overpower a Seyfert optical nuclear spectrum, given that the starburst component in these objects is not particularly strong. On the contrary here we propose that the AGN and the starburst components in these objects are present at the same level of activity making them ideal laboratories in which the two phenomena can be studied together.

Until recently little or no information in the X-ray spectral domain were available for the M96 sample of Composite galaxies except for the ROSAT data. In the last couple of years, *Chandra* and *XMM-Newton* observations of IRAS 00317–2142 and IRAS 20051–1117, two of the brightest objects of the sample, have revealed the presence of an active nucleus with a spectral shape typical of type 1 AGN's (a photon index $\Gamma \sim 1.8-1.9$) and no absorption. Long term variability has been observed in IRAS 00317–2142 (Georgantopoulos, Zezas & Ward 2003), while no flux variation has been measured

¹ Instituto de Fisica de Cantabria (CSIC-UC), Avda. de los Castros, 39005 Santander, Spain

² Center for Astrophysics, 60 Garden Street, Cambridge, MA 02138

³ Osservatorio Astronomico di Brera, Via Brera 28, 20121 Milano, Italy

⁴ Dipartimento di Astronomia, Università di Bologna, via Ranzani 1, 40127 Bologna, Italy

⁵ Istituto di Astrofisica Spaziale e Fisica Cosmica (IASF-CNR), Via Gobetti 101, 40129 Bologna, Italy

in IRAS 20051–1117 (Georgantopoulos et al. 2004).

In order to acquire the missing information in X-rays for the rest of the sample, and to derive the overall properties for the whole sample, we first proposed to observe these objects with *BeppoSAX* (Boella et al. 1997) and we obtained data for 3 sources of the original list of 6 of Moran et al. (1996). Then we observed four objects of the sample with *Chandra* (Weisskopf et al. 2000). Here we present the results obtained from the *Chandra* and *BeppoSAX* observations and discuss possible explanations for the enigmatic behaviour of this class of objects.

The paper is organized as follows: the sample is briefly outlined in Section 2, new X-ray observations are described in Sections 3 through 6 and discussed together with a multi-frequency analysis in Section 7. Our conclusions are drawn in Section 8. Throughout the paper we assume $H_0 = 75 \text{ km s}^{-1} \text{ Mpc}^{-1}$.

2. THE COMPOSITE SAMPLE

We list the 6 objects defined as Composite by M96 in Table 1. We note that the original M96’s list included 7 objects, but IRAS 10113+1736 is no longer a valid Composite, since it has become evident that infrared and X-ray emissions originate from different sources (Condon et al. 1998a).

Table 1 lists all the sample properties, i.e. J2000 position, redshift, Hubble type (from LEDA⁶, Paturel et al. 1997), Galactic N_H from Dickey & Lockman (1990), IRAS far-infrared luminosities; we also report the logarithmic luminosities of the $H\alpha$ (narrow+broader and only broader) and $[O III]\lambda 5007$ emission lines obtained by M96 in a $2'' \times 4''$ aperture.

We note that IRAS 00317–2142 belong to the compact group HCG 4. However, no extended emission is detected in the group at a limit of $10^{41} \text{ erg s}^{-1}$ in the ROSAT PSPC (Mulchaey et al. 2003), so that no group emission is expected to contaminate our results.

The galaxies are local ($z < 0.04$). They are all detected by the NVSS (Condon et al. 1998b) in the range 6–44 mJy and by the 2MASS (Cutri et al. 2003) with K_s mag between 10.3 and 11.6. Their optical magnitudes range between 14 and 16 (from NED).

For completeness we include the results of the ASCA, XMM-*Newton* and *Chandra* observations of IRAS 00317–2142 and IRAS 20051–1117 (Georgantopoulos 2000, Georgantopoulos, Zezas & Ward 2003, Georgantopoulos et al. 2004) in the X-ray table results (see Sect. 5) and in the final discussion of the whole sample.

3. X-RAY DATA

3.1. *BeppoSAX* Observations

We observed three Composite objects with the Narrow Field Instruments (NFI) of the *BeppoSAX* satellite. The observation dates and the total effective exposure time in ks for the LECS (0.1–4 keV), MECS (1.3–10 keV) and PDS (13–200 keV) instruments are listed in the bottom part of Table 2. All objects have been detected by the MECS instrument, none by the LECS detector. The only source detected by the PDS is IRAS 20051–1117 ($S/N \gtrsim 3$) with a total count rate of $(13.73 \pm 4.48) \times 10^{-2}$

cts/s in the 20–200 keV band; however the PDS data fall above the simple power-law extrapolation from the MECS data suggesting a possible contamination from a different object as discussed in Sec 4.

The extraction of the source and background spectra was done with the XSELECT package. The MECS spectra have been extracted from a 4 arcmin radii circular regions; the background for each source has been extracted from source free off-axis circular regions and subtracted. The redistribution matrices and ancillary response files released in September 1997 have been applied. MECS net count rates and errors are listed in Table 2.

3.2. *Chandra* Observations

We observed four objects with the Advanced CCD Imaging Spectrometer ACIS-I on board *Chandra* between March and September 2003 using exposures of ~ 25 ks. Details of the observations can be found in the top part of Table 2. The data reduction was performed using the CIAO version 3.1 software. Level 1 event files have been created applying the time-dependent gain correction. The standard procedure provided by the CIAO “threads” has been followed in order to obtain level 2 event files. Background light curves have been examined and in two cases (IRAS 01072+4954 and IRAS 01319–1604) background flares have been found and removed. In all cases, “good” exposure times (listed in column 3 of Table 2) are always $\geq 90\%$ of the total observation times. Based on the RASS fluxes, we had requested observations in 1/4 sub-array mode in order to minimize pile-up effects. However, we found that the observed count rates are below the expected values, therefore no pile-up affects the observations.

Nuclear spectra have been extracted from a circular region of a $3''$ radius; the background has been evaluated in nearby source free regions and, as shown by the errors on the ACIS-I net count rates (Table 2), it contributes less than few percent to the total count rate.

4. CHANDRA IMAGING ANALYSIS

We have run a detection algorithm (*wavdetect* in CIAO) in fields of view of $\sim 5' \times 2'$ of the ACIS-I3. Point-like emissions coincident with the optical position of the nucleus have been detected in all objects, confirming the X-ray/optical association.

We list the off-nuclear sources detected within the optical extent (D25) of each galaxy in Table 3. We give the positions in RA & DEC (J2000), the distance from the nucleus in arcsec and kpc, the number of net counts and relative errors, the source significance and the 2–10 keV fluxes and luminosities computed assuming a $\Gamma=1.8$ power-law spectrum modified by Galactic column densities, and the redshift of the corresponding galaxy. We do not detect any off-nuclear source within the optical extent of IRAS 01072+4954 (at the given exposure the flux limit corresponds to a luminosity of $2.5 \times 10^{39} \text{ erg/s}$). All the off-nuclear sources are significantly detected at $> 3\sigma$. If they are actually associated with the host galaxies, the observed luminosities would be well in excess of the Eddington luminosity for a solar-mass black hole or neutron star X-ray binary, therefore they should be considered as Ultra-Luminous X-ray objects (ULXs, Swartz et al. 2004). Note that despite the presence of these luminous sources, the galaxy X-ray emission is completely

⁶ <http://leda.univ-lyon1.fr/>

dominated by the nucleus in each case.

Given the large RASS point spread function of about $45''$ even for bright sources and the positional accuracy of $25''$ (90% confidence level, Voges et al. 1999), other sources could in principle contaminate the RASS detection. To verify whether any other X-ray source was present within the ROSAT aperture we examined the $\sim 2'$ region around each source. We have found a source with ≤ 50 cts at $121''$ from the nucleus of IRAS 01072+4954, a source with ≤ 15 cts at $55''$ from IRAS 01319–1604 and a source with ≤ 45 cts at $79.5''$ from IRAS 04392–0123. In the present data, these sources contribute at most 15% of the nuclear flux, so that it is unlikely that they could have been dominant in the ROSAT observations.

In order to look for extended emission, the radial profile of each source has been derived in annular regions centered on the nuclear position and reaching out to $5''$, where the signal fades into the background. We also obtained a radial profile for the *Chandra* PSF, by using the CIAO task *chart*, which simulates, by ray-tracing, a source with the same spectrum as the target and an exposure time appropriate to derive the statistics needed to define the PSF shape with virtually no errors (we choose 100 ks). After normalizing for the different exposure times, we compared the source and the *Chandra* simulated PSF, as described in the CIAO Threads, using the SHERPA software. In all cases but one, the source is consistent with a point source. In Figure 1 we show the radial profile of IRAS 01072+4954; this source is characterized by the presence of faint extended emission between $1'' - 3''$ from the center, which correspond to a region of 0.5-1.3 kpc (at the redshift of the source). This effect is more pronounced in the soft (0.3-2 keV) than in the hard (2-10 keV) energy band.

5. SPECTRAL ANALYSIS

Both *Chandra* and *BeppoSAX* spectral data have been grouped to at least 20 counts per bin and spectra in the range of 0.3-10 keV have been analyzed using the XSPEC software package. We first fitted *Chandra* and *BeppoSAX* spectra separately. Each spectrum has been initially fitted with a single power-law plus Galactic absorption. In all objects this simple parametrization describes well the observed spectra and the spectral shapes are within the typical ranges observed for AGNs, i.e. photon indices from 1.7 and 2, except for IRAS 04392–0123 which shows a flatter spectrum ($\Gamma \sim 1.3$) both in *Chandra* and *BeppoSAX* observations. Intrinsic absorption values, when measured, are of the order of 10^{21} cm^{-2} or slightly in excess of the Galactic value (Dickey & Lockman, 1990). In the case of the flat spectrum of IRAS 04392–0123, the upper limit derived on the column density ($N_H < 6 \times 10^{20} \text{ cm}^{-2}$) remains consistent with the Galactic absorption even when fixing the spectral slope to the AGN canonical value ($\Gamma = 1.9$).

BeppoSAX spectral results are listed in Table 4. Although at lower significance, the *BeppoSAX* spectral parameters are in agreement within the errors with those derived from the *Chandra* data. We have therefore fitted all the available data for the same source together. The final spectra are plotted in Figure 2 while the spectral results are presented in Table 5. We also report the results from Georgantopoulos, Zezas & Ward (2003), Geor-

giantopoulos et al. (2004) in the same table for ease of reference. The quoted errors on the spectral parameters correspond to the 90% confidence level for one interesting parameter.

We discuss here each source in turn. IRAS 20051–1117 is the brightest source of the sample observed by *BeppoSAX*. Its spectrum is well described by a simple power-law, with a photon index ($\Gamma \sim 1.9$) in agreement with the one reported by Georgantopoulos et al. (2004), using *Chandra* and XMM-*Newton* data. The addition of a Gaussian component consistent with an FeK α line (at $6.29_{-0.48}^{+0.28}$ keV, rest frame) is significant at only 2σ ($\text{EW} = 282_{-214}^{+215}$ eV), again in agreement with Georgantopoulos et al. (2004) *Chandra* results. Residuals are also present around 6.9 keV (see Figure 2) but at a lower statistical significance. At high energies (13-200 keV), the PDS data fall above the simple power-law extrapolation from the MECS (1.3-10 keV), by a factor of ~ 5 . We explored the $\sim 1^\circ$ region around the target to look for possible contaminant sources. We found 1RXS J200433.5-111345, detected by RASS at $\sim 50'$ from IRAS 20051–1117 and brighter by a factor 1.3, corresponding to a galaxy detected by IRAS (no other relevant information like redshift, morphological classification, etc. is available). The source could be the contaminant if it hosts an absorbed nucleus. Given the discrepancy in the relative fluxes, the partial contamination from 1RXS J200433.5-111345 or other sources is likely, and therefore we make no further use of the PDS spectrum. On the other hand a Compton thick AGN in IRAS 20051–1117 is ruled out by the lack of a FeK line with high EW (see below).

IRAS 01072+4954 and IRAS 04392–0123 have been observed by both *Chandra* and *BeppoSAX*. In Figure 2 we show *Chandra* and *BeppoSAX* spectra fitted simultaneously leaving the relative normalization free to vary. Their values are in the range 1-1.3, indicating that the *Chandra* and *BeppoSAX* normalizations are within 30%, that would either indicate a minimal flux variation between the two observations, or the uncertainty in the relative calibration between instruments.

In the *Chandra* spectrum of IRAS 01072+4954 a thermal component (MEKAL) has been added to the model to account for residuals visible below 2 keV above the simple power law. Such component has a 0.3-2 keV flux of $4.6 \times 10^{-14} \text{ erg cm}^{-2} \text{ s}^{-1}$ ($L_{0.3-2\text{keV}} \sim 5.8 \times 10^{40} \text{ erg s}^{-1}$) and it is significant at 99.99% (via an F-test), consistently with the presence of the faint extended soft component revealed by its radial profile.

IRAS 20069+5929 has the highest fitted value for intrinsic N_H , which is however still consistent with absorption from the host galaxy.

The presence of an Fe line at 6.4 keV is not statistically significant in any of the sources observed by *Chandra*. In the case of IRAS 00317–2142 and IRAS 01072+4954 the upper limit to the equivalent widths at 90% (as shown in Table 5) is not stringent, due to the poor statistics above 6 keV. In the other cases, the upper limits are always consistent with expectation from the low intrinsic absorption measured, ruling out the Compton thick hypothesis (Bassani et al. 1999).

6. TIMING ANALYSIS

6.1. Short-term variability

The ACIS-I light curves have been examined in order to look for short term variability. In Figure 3 we show the 0.3-10 keV Chandra light curves of all sources. They have been extracted from circular regions of $3''$ radius, binned at 1 ks and fitted with a constant. The resulting constant values and χ^2/dof are given in Table 6 for the 0.3-10 keV, 0.3-2 keV and 2-10 keV energy ranges. In the cases of IRAS 01072+4954, IRAS 01319–1604 and IRAS 20069+5929 the hypothesis of a constant flux is rejected at the 99% confidence level. In particular, IRAS 01072+4954 and IRAS 01319–1604 show larger flux variations in the soft X-ray band. To illustrate this point, in Figure 4 we plot the soft and hard light curves for IRAS 01319–1604, the most variable source of the sample. The non-detection of variability in IRAS 04392–0123 is possibly due to the low statistics available. We examine also the *BeppoSAX* light curve of IRAS 20051–1117 (see Fig. 5), in bin sizes of 3 ks. Fitting a constant to the observed count rate we reject the constant flux hypothesis at more than 95% level (see Table 6). However, *Chandra* or XMM-*Newton* short-term light curves show no variability either in this source (Georgantopoulos et al. 2004), nor is detected in *Chandra* for IRAS 00317–2142 (Georgantopoulos, Zezas & Ward 2003). The variability of a factor 2-3 for IRAS 20051-1117 over a time scale of ~ 4 ks implies (using light crossing arguments) that the dimensions of the emitting region are typical of a nuclear source ($\leq 1.2 \times 10^{14}$ cm, i.e. 4×10^{-5} pc).

When the statistics allows it, we have attempted to extract the spectrum at different intervals to check for possible spectral variations, suggested by the higher variability measured in the soft band. However, the spectral parameters measured in the different states (high and low flux) are always consistent within errors.

6.2. Long-term variability

In order to examine the presence of long-term variability we compared the observed fluxes from all available X-ray measurements, both from literature and from our *BeppoSAX* and *Chandra* data presented here. Figure 6 shows the long term light curves for the six sources in the sample. Errorbars have been plotted for all the fluxes except those derived from the literature for which errors on the count rates were not available. For a better comparison, all ROSAT, *BeppoSAX* and *Chandra* 0.3-2 keV fluxes have been recomputed, assuming the *Chandra* best fit spectral shape as reported in Table 5. The resulting 0.3-2 keV unabsorbed fluxes are given in Table 7. All our sources have been observed by the ROSAT All-Sky Survey (RASS) with the Position Sensitive Proportional Counter (PSPC) in the 0.1-2.4 energy band. The RASS count rates and errors have been taken from Boller et al. (1992). IRAS 00317–2142 and IRAS 01319–1604 have also been observed in a PSPC pointed observation. In the 2 yr period between the RASS and the PSPC pointed observation, IRAS 00317–2142 does not show significant variability while IRAS 01319–1604 has nearly doubled its flux (measured by the same instrument). ASCA and *Chandra* count rates of IRAS 00317–2142 have been taken from Georgantopoulos (2000) and Georgantopoulos, Zezas & Ward (2003), respectively. In the case of IRAS 20051–1117, *Chandra* and XMM-*Newton* count rates, taken from Georgantopoulos et al. (2004),

were both obtained on 2002 April 1 and the measured soft fluxes are comparable within a few percent; therefore we only consider the *Chandra* data for the long-term analysis.

Unfortunately, the statistics in the ROSAT observations is not sufficient to derive a reliable spectral measurement, therefore a possible spectral variation could have occurred between the ROSAT and the *BeppoSAX*/*Chandra* epochs, even if we do not observe spectral variability between the *BeppoSAX* and *Chandra* observations. While we do not observe flux variations on time scales of ~ 2 yr between the *BeppoSAX* and the *Chandra* observations, IRAS 04392–0123 has experienced a variation by a factor of ~ 24 in ~ 10 yr between the ROSAT and the *Chandra* observations, similarly to the case of IRAS 00317–2142 which varied by a factor of ~ 20 (see also Georgantopoulos, Zezas & Ward, 2003). Also IRAS 01072+4954 and IRAS 01319–1604 varied, even though only by a factor of ~ 3 . The strong long term variability in the X-rays seems very common in this class.

7. DISCUSSION

The X-ray analysis of Composite galaxies has revealed their AGN dominance in this spectral domain.

In what follows we make use of various diagnostic diagrams and multi-frequency data to investigate the reasons for the contradictory optical/X-ray classification of these objects, and suggest a global explanation of the phenomenon.

7.1. Diagnostic Diagrams

The optical diagnostic diagrams obtained using standard emission line ratios (Veilleux & Osterbrock, 1987) show that Composites are very close to the boundary region between starbursts and AGNs confirming the M96 classification. This is shown in Figure 7 where the $[O III]/H\beta$ ratio is plotted vs. the $[NII]/H\alpha$ (the other two standard diagnostics which make use of $[SII]/H\alpha$ and $[OI]/H\alpha$ ratios give similar results). The lines represent the theoretical starburst limits, a standard one which have been taken from Kewley et al. (2001) (together with the dotted lines which indicate the error range) and an updated estimate for the starburst boundary derived from the SDSS observations (from Kauffmann et al. 2003). The location of the ‘Composite’ region should be between these two lines (Hornschemeier et al. 2005).

However, when the flux of the optical emission line $[O III]\lambda 5007$ is combined with the infrared and X-ray fluxes, Composite galaxies are classified as AGNs rather than starburst. In Figure 8 the diagram with the combination of $F_X/F_{[O III]}$ vs. $F_{[O III]}/F_{IR}$ ratios is shown. These flux ratios have been used to separate the AGN and the starbursts contributions by Panessa & Bassani (2002) and Braito et al. (2004), based on the fact that the $[O III]\lambda 5007$ flux is associated with the AGN and the far-infrared emission is associated mainly with the star-forming activity. At the same time they are a powerful tool in the detection of heavy obscuration not seen in X-rays below 10 keV (as in Compton thick objects, Bassani et al. 1999). Clearly Composite objects all fall in the AGN region, in good agreement with the relative broadness of the $[O III]\lambda 5007$ line found by M96 which points to an AGN origin. The diagram further shows that they

should all be classified as Compton thin AGN (note that the X-ray fluxes used in the plot are those observed in the ‘low-state’ epoch, and therefore the classification would be also valid in the ‘high-state’). This indicates very little amount of absorption, in agreement with the results obtained from the X-ray analysis, i.e. the absence of a strong Fe-line and X-ray obscuration. Therefore the relative weakness of the AGN optical emission lines cannot be explained as due to the presence of absorbing material in the line of sight, as suggested by M96.

7.2. X-ray vs. infrared luminosity diagram

Having assessed the importance of the AGN component from the X-ray, infrared and [O III] emissions combined, we want to estimate here the amount of X-ray emission expected to be produced by the presence of a starburst. Therefore we derived the Star Formation Rate (SFR) from the far-infrared luminosity (Kennicutt 1998), assuming that the latter (given in Table 1) is all due to the starburst. The SFRs obtained are in the range of 5-34 M_{\odot}/yr (note that these values are upper limits since we have not subtracted the possible AGN contribution from the FIR luminosity). Subsequently, the L_X in the 2-10 keV band associated to the derived SFRs have been estimated as in Nandra et al. (2002), Grimm et al. (2003), Ranalli et al. (2003), Persic et al. (2004). The derived correlations have been plotted in Figure 9, together with the observed hard L_X vs. L_{FIR} for each Composite object. For all sources, regardless of the correlation considered, the X-ray observed emission is well above the value expected to be produced by a starburst. The SFR derived here for the Composites correspond to a starburst that is not bright enough to produce the observed X-ray emission, which is then mostly given by the AGN, as suggested by our X-ray analysis. Observed X-ray emission in excess to that predicted from SFR has also been observed in high-redshift submillimeter sources (Alexander et al. 2003), that might point to the presence of an active nucleus also for this class of objects. Only in the case of IRAS 00317–2142 the observed X-ray luminosity is close to the expected value for a starburst; this is in agreement with the results of the multi-wavelength analysis for this object presented in the next Section.

7.3. Spectral Energy Distributions

Spectral Energy Distributions (SEDs) have been assembled from radio ($\nu \approx 10^8$ Hz) to hard X-rays ($\nu \approx 10^{18}$ Hz) for our sample sources. Radio, far to near infrared, optical, X-ray data have been taken from NED, and complemented with the *Chandra* data from this work. All X-ray data points have been plotted with the spectral shape measured in the *Chandra* observations.

In Figure 10 we compare the observed SEDs with the templates of Medium Energy Distribution for radio quiet quasars (Elvis et al. 1994), starburst galaxies (Schmitt et al. 1997) and normal spiral galaxies (Elvis et al. 1994). The templates we show are normalized to match, and not exceed data points. In particular, the starburst template is normalized to the radio-IR portion of the spectrum, while the X-ray one is normalized to the different X-ray states observed. We stress that we are only interested in deriving an overall consistent picture, without attempting a quantitative computation of the contributions of

the different components, that would require at least simultaneous data to account for the observed variability in the X-ray band. Moreover, it must be taken into account that all data points have been taken using different apertures, in particular for the optical band where the emission is heavily contaminated by the host galaxy. The SEDs show clearly the *Composite* nature of these objects: the AGN dominates at X-ray wavelengths, while the starburst is the most important contributor to the mid/far IR emission; the host galaxy template accounts for the optical appearance.

It is evident that, in the optical band, the AGN contribution is always less than that of the starburst, and, except for a couple of sources during their ‘high’ state, even by a factor of 10. Note instead that in IRAS 00317–2142, when it is in the low state, the contributions to the X-ray emission from the AGN and the starburst become comparable (in agreement with Figure 9).

The AGN contributes to the total bolometric luminosity from less than 10% in the ‘low flux state’, to 15-30% in the ‘high flux state’ thus making the SB contribution dominant in the bolometric output, except possibly during bright AGN flares.

Mid-infrared and L-band spectroscopy could provide a powerful way to disentangle the starburst from the AGN component (Genzel et al. 1998, Imanishi 2002, Risaliti et al. 2003, Lutz et al. 2003). Moreover broad band data from the near to the far-infrared frequencies could provide a more detailed characterization of the SEDs, in particular by exploiting the Spitzer Space Telescope unprecedented capabilities (see e.g. Franceschini et al. 2005).

7.4. A weak and low M_{BH} AGN?

IRAS 00317–2142, IRAS 20051–1117 and IRAS 20069+5929 are the only three sources for which a weak broad component of the $H\alpha$ emission line has been detected in their optical spectra, while in all objects the narrow $H\alpha$ component is probably due to the starburst. A correlation between the 2-10 keV X-ray luminosity versus the $H\alpha$ luminosity has been widely observed in high and low luminosity AGNs (Ward et al. 1988, Ho et al. 2001). IRAS 00317–2142, IRAS 20051–1117 and IRAS 20069+5929, for which we consider only the broad $H\alpha$ components, follow the Ho et al. (2001) correlation (which applies to both high and low luminosity AGNs). The remaining three Composites for which the broad $H\alpha$ was not measured are generally fainter both in X-rays and in the optical band; therefore it is likely that an optical emission line luminosity of a factor of 2-3 lower could be difficult to measure. Using the Kennicutt (1998) relation, we derived the SFR from the $H\alpha$ luminosity produced by the narrow component and we estimated the expected 2-10 keV luminosity to be produced by that SFR (Ranalli et al. 2003). The expected 2-10 keV luminosities are in the range of 10^{39-40} erg s^{-1} , i.e. a factor of 50-100 lower than the observed ones. This result is consistent with our previous interpretation that in all objects the narrow $H\alpha$ component is probably due to the starburst, and the X-rays to the AGN.

For the three objects for which we have a measure of the broad $H\alpha$ component, we attempt an estimate of the

Black Hole Mass. We make use of the formula $M_{BH} = v^2 R_{BLR}/G$ (McLure & Dunlop 2001) and of a few additional assumptions. The quantities $v = 1.5 FWHM H\beta$ and $R_{BLR} = 32.9(\lambda L_{5100}/10^{44} \text{ erg s}^{-1})^{0.7}$ in light days (Kaspi et al. 2000) require a measure of the broad $H\beta$ emission, which is not detected because swamped by the narrow line produced by the starburst and of the AGN continuum, which we do not measure directly. We substitute the FWHM of $H\beta$ with the FWHM of the broad $H\alpha$ that we attribute to the AGN (from M96). If anything, the $H\alpha$ is usually broader than $H\beta$, therefore we will overestimate the resulting mass. We infer the AGN continuum from the template fitted to the X-ray luminosity. This is a rough approximation of the real illuminating continuum, but it should be correct within an order of magnitude at least. Plugging these numbers in the above formula we derive numbers for the mass of the order of a few $10^{5-6} M_{\odot}$. An order of magnitude uncertainty on the $L_{5100, A}$ changes the mass by $10^{0.7}$. We therefore can conclude that most probably the masses of these black holes are small and that they could possibly undergo strong changes in accretion rate when they brighten. We have found a possible analogy between our sources and the Seyfert 1.5 NGC 4395. It is a low luminosity AGN with a small black hole mass, that shows X-ray variability, although more violent than what observed in the Composites (Vaughan et al. 2005).

The Black Hole Mass range is consistent with all these objects being late type galaxies (as indicated by their morphological types in Table 1) with small stellar bulges. In fact, from their total B-band magnitude and an average bulge/total flux ratio typical of their morphological type (de Jong 1996), we derived the black hole mass values which are consistent with those previously found, when assuming that the $L_{B, bulge} - M_{BH}$ correlation (e.g., Yu & Tremaine 2002) still holds for late type spirals.

Detailed follow up observations (e.g. high spatial resolution optical spectroscopy) are needed in order to provide a more reliable estimate of the black hole mass for these objects.

8. CONCLUSIONS

New *Chandra* and *BeppoSAX* observations of 4 and 3 Composites, respectively, have deepened our knowledge of this class of sources. Based on the X-ray analysis presented here, Composite galaxies behave like typical type 1 AGNs in the X-ray band: their emission is dominated by a bright nuclear source, whose spectral properties are typical of this class. A power-law model with spectral index ($\Gamma = 1.7-2.1$) and little intrinsic absorption ($N_H < 4 \times 10^{21} \text{ cm}^{-2}$) well describe their spectra. Iron lines are not significantly detected (upper limits on their equivalent widths are below $\sim 400 \text{ eV}$). Large flux variability is found on many different temporal scales.

A broad analysis of the whole Composite sample, carried out by adding to our X-ray data the results from Georgantopoulos (2000), Georgantopoulos, Zezas & Ward (2003), Georgantopoulos et al. (2004) and multi-wavelength data from the literature, has revealed that the study of this class is relevant both for the investigation of the AGN-starburst connection and for the X-ray properties in medium/low luminosity AGNs.

Interestingly enough, AGN and starburst activity seem to be present with almost the same intensity in this class

of objects. Spectral Energy Distributions have clearly shown that the different emission components contribute to different spectral energy bands: the infrared emission is probably dominated by the starburst and the X-ray one derives from the AGN. The optical continuum is mainly contaminated by the host galaxy light while the emission line spectrum shows narrow emission lines produced by starburst. The $H\alpha$ emission line is probably associated to both: the narrow component to the starburst and the broad component, when bright enough to be detected, correlates well with the hard X-ray luminosity, and therefore is to be ascribed to photoionization by the AGN.

It is unlikely that heavy obscuration that could explain the weakness of the AGN in the optical band is present, as shown by the pronounced X-ray variability and low column densities and by the flux diagnostic diagrams shown in section 7.1. A dusty clumpy ionized absorber, able to selectively obscure the optical emission, that leaves the X-ray emission almost unabsorbed (Georgantopoulos 2000; Maiolino et al. 2001) is clearly possible. However the detection of broad $H\alpha$ with FWHM typical of type 1 objects makes this hypothesis remote. In conclusion, the lack of clear indications of the presence of an AGN in the optical spectra of the Composites is probably due to a combination of the faintness of the AGN itself and of the masking effect of the starburst.

As mentioned above, the most striking characteristic of Composite galaxies is the strong, long- and short-term, X-ray variability observed. ROSAT observation taken between 1991 and 1992 reveal bright soft nuclei at the level of 10^{42-43} erg/s . *Chandra* and *BeppoSAX* observations taken nearly 10 years later reveal that, in most cases, these objects are fainter. Two objects show a variation in flux by a factor of 20, while in two other objects the fluxes decreased by a factor of 2-3. It is likely that the inclusion of these sources in the RASS-IRAS correlation of M96 is partly due to their bright state at that time. What is the cause for their brightening? Are they now fading away or just changing state every once in a while?

Concerning the flux variation of a factor of ~ 20 over ~ 10 yrs, we cannot say much: it is not an extreme value, but certainly not the most common (see eg. Ulrich et al 1997). Furthermore, the data sampling is very scanty and does not allow us to determine the time dependence of the variability. On the contrary, the flux variability on short time scales, with variations by a factor of 2-3 on time scales of ~ 4 ks, coupled to an estimate of low values for the central black hole mass (even though based more on assumptions than on measurements), could fit with the observed trend of higher variability for smaller black hole masses, and could also be linked to variations in the accretion rate (O'Neill et al. 2005, Mushotzky et al. 1993).

Even if small, this sample has a statistically sound definition that makes results applicable to other candidates. We cannot estimate their space density, however we notice that several examples of objects with similar characteristics have already appeared in the literature (Griffiths et al. 1996, Della Ceca et al. 2001, Guainazzi et al. 2000), which suggests that they might constitute a non-negligible fraction of the AGN family.

We therefore suggest the use of a combination of diag-

nostic ratios, such as those based on the [OIII]/FIR ratio and the presence of X-ray emission to pinpoint members of this class of Composites. New Spitzer Space Telescope and *Chandra* data would be of crucial importance to deepen our knowledge on the Composite sample and to enlarge the number of candidates belonging to the same class.

FP warmly thanks for hospitality the Center for Astrophysics where much of this work has been realized. We thank the anonymous referee for providing useful comments. We acknowledge the contribution of Massimo Cappi and Mauro Dadina for an earlier involvement in the paper, Raffaella Landi for her help with the

PDS data, Jonathan McDowell for the SED-making program *TIGER*, Martin Elvis, and Andreas Zezas for useful comments. This work has been supported by the NASA grants GO3-4131X and NAS8-39073 to the *Chandra* X-Ray Center. This work has received partial financial support by ASI and Cofin Miur. RDC acknowledge partial financial support from the MIUR (Cofin-03-02-23). This research makes use of the NASA/IPAC Extra-galactic Database (NED) and of data products from the Two Micron All Sky Survey, which is a joint project of the University of Massachusetts and the infrared Processing and Analysis Center/California Institute of Technology, funded by the National Aeronautics and Space Administration and the National Science Foundation.

REFERENCES

- Alexander, D. M., et al. 2003, *AJ*, 125, 383
 Bassani, L., Dadina, M., Maiolino, R., Salvati, M., Risaliti, G., della Ceca, R., Matt, G., & Zamorani, G. 1999, *ApJS*, 121, 473
 Boella, G., Butler, R. C., Perola, G. C., Piro, L., Scarsi, L., & Bleeker, J. A. M. 1997, *A&AS*, 122, 299
 Boller, T., Meurs, E. J. A., Brinkmann, W., Fink, H., Zimmermann, U., & Adorf, H.-M. 1992, *A&A*, 261, 57
 Braitto, V. et al. 2004, Proceedings of the VI Italian Conference on Active Galactic Nuclei, <http://www.arcetri.astro.it/~agn6/>
 Comastri, A., et al. 2002, *ApJ*, 571, 771
 Condon, J. J., Yin, Q. F., Thuan, T. X., & Boller, T. 1998a, *AJ*, 116, 2682
 Condon, J. J., Cotton, W. D., Greisen, E. W., Yin, Q. F., Perley, R. A., Taylor, G. B., & Broderick, J. J. 1998b, *AJ*, 115, 1693
 Cutri, R. M., et al. 2003, *VizieR Online Data Catalog*, 2246, 0
 David, L. P., Jones, C., & Forman, W. 1992, *ApJ*, 388, 82
 de Jong, R. S. 1996, *A&A*, 313, 45
 Della Ceca, R., Pellegrini, S., Bassani, L., Beckmann, V., Cappi, M., Palumbo, G. G. C., Trinchieri, G., & Wolter, A. 2001, *A&A*, 375, 781
 Dickey, J. M., & Lockman, F. J. 1990, *ARA&A*, 28, 215
 Elvis, M. et al., 1994, *apjs*, 95, 1
 Fabian, A. C., Barcons, X., Almaini, O., & Iwasawa, K. 1998, *MNRAS*, 297, L11
 Ferrarese, L., & Merritt, D. 2000, *ApJ*, 539, L9
 Franceschini, A. et al. 2005, Accepted for publication in *AJ*, March 2005 issue, astro-ph/0412476
 Genzel, R., et al. 1998, *ApJ*, 498, 579
 Georgantopoulos, I., Papadakis, I., Zezas, A., & Ward, M. J. 2004, *ApJ*, 614, 634
 Georgantopoulos, I., Zezas, A., & Ward, M. J. 2003, *ApJ*, 584, 129
 Georgantopoulos, I. 2000, *MNRAS*, 315, 77
 González Delgado, R. M., Heckman, T., & Leitherer, C. 2001, *ApJ*, 546, 845
 Griffiths, R. E., della Ceca, R., Georgantopoulos, I., Boyle, B. J., Stewart, G. C., Shanks, T., & Fruscione, A. 1996, *MNRAS*, 281, 71
 Grimm, H.-J., Gilfanov, M., & Sunyaev, R. 2003, *MNRAS*, 339, 793
 Guainazzi, M., Dennefeld, M., Piro, L., Boller, T., Rafanelli, P., & Yamauchi, M. 2000, *A&A*, 355, 113
 Ho, L. C. et al. 2001, *ApJ*, 549, L51
 Hornschemeier, A. E., Heckman, T. M., Ptak, A. F., Tremonti, C. A., & Colbert, E. J. M. 2005, *AJ*, 129, 86
 Imanishi, M. 2002, *ApJ*, 569, 44
 Kaspi, S., Smith, P. S., Netzer, H., Maoz, D., Jannuzi, B. T., & Giveon, U. 2000, *ApJ*, 533, 631
 Kauffmann, G., et al. 2003, *MNRAS*, 346, 1055
 Kennicutt, R. C. 1998, *ApJ*, 498, 541
 Kewley, L. J., Heisler, C. A., Dopita, M. A., & Lumsden, S. 2001, *ApJS*, 132, 37
 Kormendy, J., Bender, R., & Bower, G. 2002, *Astronomical Society of the Pacific Conference Series*, 273, 29
 Levenson, N. A., Weaver, K. A., Heckman, T. M., Awaki, H., & Terashima, Y. 2004, *ApJ*, 602, 135
 Levenson, N. A., Fernandes, R. C. J., Weaver, K. A., Heckman, T. M., & Storchi-Bergmann, T. 2001, *ApJ*, 557, 54
 Lutz, D., Sturm, E., Genzel, R., Spoon, H. W. W., Moorwood, A. F. M., Netzer, H., & Sternberg, A. 2003, *A&A*, 409, 867
 Maiolino, R., Marconi, A., & Oliva, E. 2001, *A&A*, 365, 37
 McLure, R. J., & Dunlop, J. S. 2001, *MNRAS*, 327, 199
 Moran, E. C., Halpern, J. P., & Helfand, D. J. 1996, *ApJS*, 106, 341
 Mulchaey, J. S., Davis, D. S., Mushotzky, R. F., & Burstein, D. 2003, *ApJS*, 145, 39
 Mushotzky, R. F., Done, C., & Pounds, K. A. 1993, *ARA&A*, 31, 717
 Nandra, K., Mushotzky, R. F., Arnaud, K., Steidel, C. C., Adelberger, K. L., Gardner, J. P., Teplitz, H. I., & Windhorst, R. A. 2002, *ApJ*, 576, 625
 Nipoti, C., Londrillo, P., & Ciotti, L. 2003, *MNRAS*, 342, 501
 Ohsuga, K. & Umemura, M. 2001, *ApJ*, 559, 157
 O'Neill P. M. et al. 2005, astro-ph/0501471
 Panessa, F., & Bassani, L. 2002, *A&A*, 394, 435
 Persic, M., Rephaeli, Y., Braitto, V., Cappi, M., Della Ceca, R., Franceschini, A., & Gruber, D. E. 2004, *A&A*, 419, 849
 Paturel, G., et al. 1997, *A&AS*, 124, 109
 Ranalli, P., Comastri, A., & Setti, G. 2003, *A&A*, 399, 39
 Risaliti, G., et al. 2003, *ApJ*, 595, L17
 Sazonov, S. Y., Ostriker, J. P., Ciotti, L., & Sunyaev, R. A. 2005, *MNRAS*, 358, 168
 Schmitt, H. R., Kinney, A. L., Calzetti, D., & Storchi Bergmann, T. 1997, *AJ*, 114, 592
 Springel, V., Di Matteo, T., & Hernquist, L. 2005, *ApJ*, 620, L79
 Swartz, D. A., Ghosh, K. K., Tennant, A. F., & Wu, K. 2004, *ApJS*, 154, 519
 Ulrich, M., Maraschi, L., & Urry, C. M. 1997, *ARA&A*, 35, 445
 Vaughan, S., Iwasawa, K., Fabian, A. C., & Hayashida, K. 2005, *MNRAS*, 356, 524
 Veilleux, S. 2001, *starburst Galaxies: Near and Far*, 88
 Veilleux, S., & Osterbrock, D. E. 1987, *ApJS*, 63, 295
 Ward, M. J., Done, C., Fabian, A. C., Tennant, A. F., & Shafer, R. A. 1988, *ApJ*, 324, 767
 Weisskopf, M. C., Tananbaum, H. D., Van Speybroeck, L. P., & O'Dell, S. L. 2000, *Proc. SPIE*, 4012, 2
 Yu, Q., & Tremaine, S. 2002, *MNRAS*, 335, 965

TABLE 1
THE COMPOSITE SEYFERT/STAR-FORMING SAMPLE

Name	RA (J2000)	DEC (J2000)	z	Hubble Type	$N_{\text{H}}^{\text{Gal}}$ 10^{20} cm^{-2}	Log L(FIR)	Log $L_{\text{H}\alpha}^{\text{Tot}}$	Log $L_{\text{H}\alpha}^{\text{Broad}}$	Log $L_{[\text{O III}]}$
IRAS 00317–2142	00:34:13.8	–21:26:21	0.0268	Sbc	1.55	44.87	41.41	41.04	41.11
IRAS 01072+4954	01:10:14.1	+50:10:32	0.0237	Sc	15.1	44.09	40.64	–	40.70
IRAS 01319–1604	01:34:25.1	–15:49:08	0.0199	Sb	1.42	44.29	40.76	–	40.89
IRAS 04392–0123	04:41:48.2	–01:18:06	0.0289	Sc	5.43	44.26	40.71	–	41.01
IRAS 20051–1117	20:07:51.3	–11:08:35	0.0315	–	6.53	44.88	41.01	40.67	41.44
IRAS 20069+5929	20:07:50.8	+59:38:10	0.0374	Sc	12.7	44.40	41.37	41.01	41.52

TABLE 2
CHANDRA ACIS-I AND *BeppoSAX* TARGET OBSERVATION DETAILS

Name	Obs. Date	Exp. (ks)			Cts/s(0.3-10 keV) (10^{-2})	
		ACIS-I			ACIS-I	
IRAS 01072+4954	2003-09-17	22.19			5.34±0.28	
IRAS 01319-1604	2003-09-20	22.77			10.20±0.37	
IRAS 04392-0123	2003-03-25	23.58			1.43±0.10	
IRAS 20069+5929	2003-03-23	23.95			17.79±0.29	
		LECS	MECS	PDS	(MECS)	
IRAS 01072+4954	2002-01-02	11.65	21.00	8.69	0.32±0.06	
IRAS 04392-0123	2001-09-14	26.32	57.38	26.81	0.26±0.03	
IRAS 20051-1117	2001-10-29	10.80	56.06	24.40	3.02±0.17	

TABLE 3
OFF-NUCLEAR SOURCES DETECTED BY *Chandra*.

Galaxy Name	X-ray	Position	Offset	Cts±Err	σ	$F_{2-10keV}$	Log $L_{2-10keV}$
	RA	DEC	(" / kpc)			10^{-15} cgs	
IRAS 01319-1604	ulx-1	01:34:25.7 -15:49:02.6	9.7/3.9	12.7±4.0	4.2	3.8	39.43
	ulx-2	01:34:24.5 -15:49:10.8	10.6/4.3	9.6±3.5	3.2	2.9	39.32
IRAS 04392-0123	ulx-1	04:41:47.6 -01:17:43.9	24.3/14.1	7.8±2.8	3.9	2.4	39.56
IRAS 20069+5929	ulx-1	20:07:51.4 +59:38:11.8	5.2/3.9	18.6±5.6	4.0	6.3	40.20

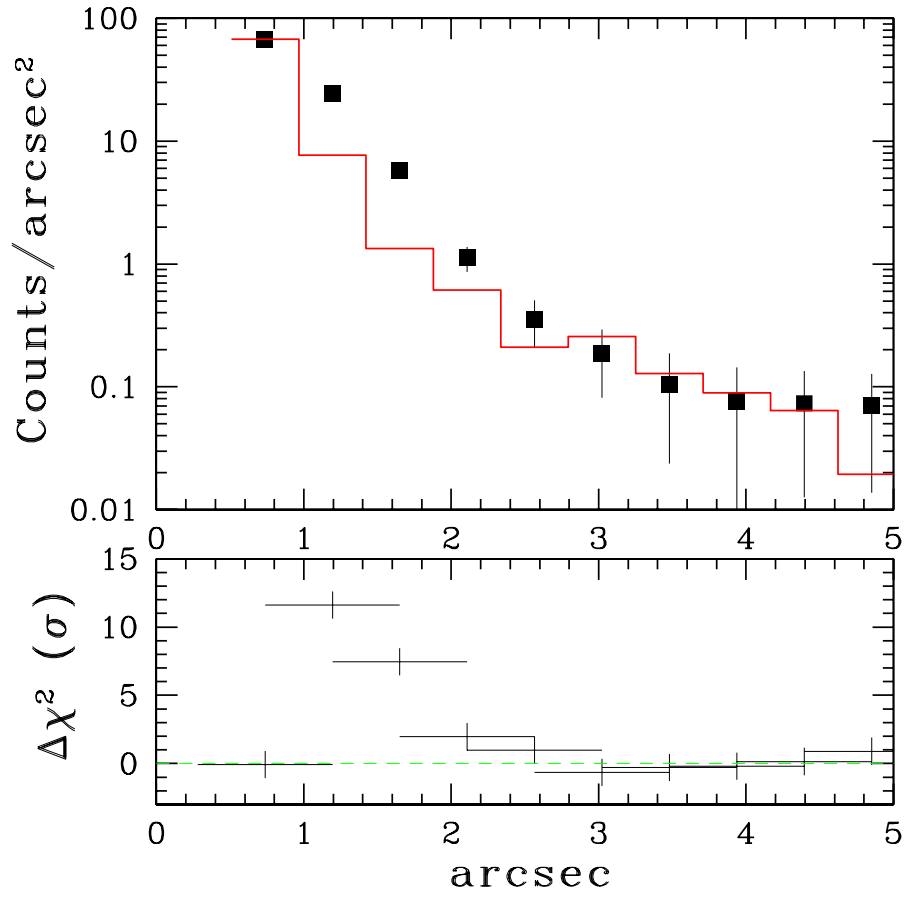


FIG. 1.— IRAS 01072+4954 radial profile (0.3-10 keV band) extracted from an annular region with 10 annuli within 5". The solid line represents the *Chandra* PSF simulated via *Chart*.

TABLE 4
BeppoSAX SPECTRAL RESULTS.

Name	N_H^{Gal} $10^{20} cm^{-2}$	N_H^{Int} $10^{22} cm^{-2}$	Γ	χ^2/dof	$F_{2-10keV}$ 10^{-12} cgs	$L_{2-10keV}$ Log
IRAS 01072+4954	15.1	<5.92	$1.87^{+2.43}_{-0.85}$	2.3/8	0.27	41.44
IRAS 04392-0123	5.43	<1.92	$1.41^{+0.80}_{-0.37}$	4/7	0.25	41.57
IRAS 20051-1117	6.53	<0.12	$1.89^{+0.09}_{-0.10}$	105/99	2.40	42.63

NOTE. — Unabsorbed fluxes and intrinsic luminosities are reported.

TABLE 5
 SPECTRAL RESULTS FOR THE TOTAL SAMPLE FROM THE COMBINED *Chandra* AND *BeppoSAX* DATA.

Name	N_H^{Gal} $10^{20} cm^{-2}$	kT keV	N_H^{Int} $10^{22} cm^{-2}$	Γ	EW eV	χ^2/dof	$F_{2-10keV}$ 10^{-12} cgs	$L_{2-10keV}$ Log
IRAS 00317-2142 ^a	1.55	-	$0.08^{+0.03}_{-0.03}$	$1.91^{+0.17}_{-0.15}$	<1400	47.3/49	0.27	41.55
IRAS 01072+4954	15.1	$0.82^{+0.17}_{-0.15}$	<0.04	$2.09^{+0.13}_{-0.15}$	<1170	56.5/66	0.31	41.49
IRAS 01319-1604	1.42	-	<0.03	$1.85^{+0.06}_{-0.07}$	<298	123.7/120	0.69	41.69
IRAS 04392-0123	5.43	-	$0.17^{+0.2}_{-0.13}$	$1.34^{+0.28}_{-0.21}$	-	15.8/20	0.19	41.46
IRAS 20051-1117 ^b	6.53	-	<0.02	$1.79^{+0.04}_{-0.04}$	250 ± 155	283.6/201	1.61	42.46
IRAS 20069+5929	12.7	-	$0.36^{+0.06}_{-0.04}$	$1.71^{+0.08}_{-0.09}$	<213	194.7/187	2.15	42.74

NOTE. — Unabsorbed fluxes and intrinsic luminosities are reported.

^aGeorgantopoulos, Zezas & Ward (2003)

^bGeorgantopoulos et al. (2004)

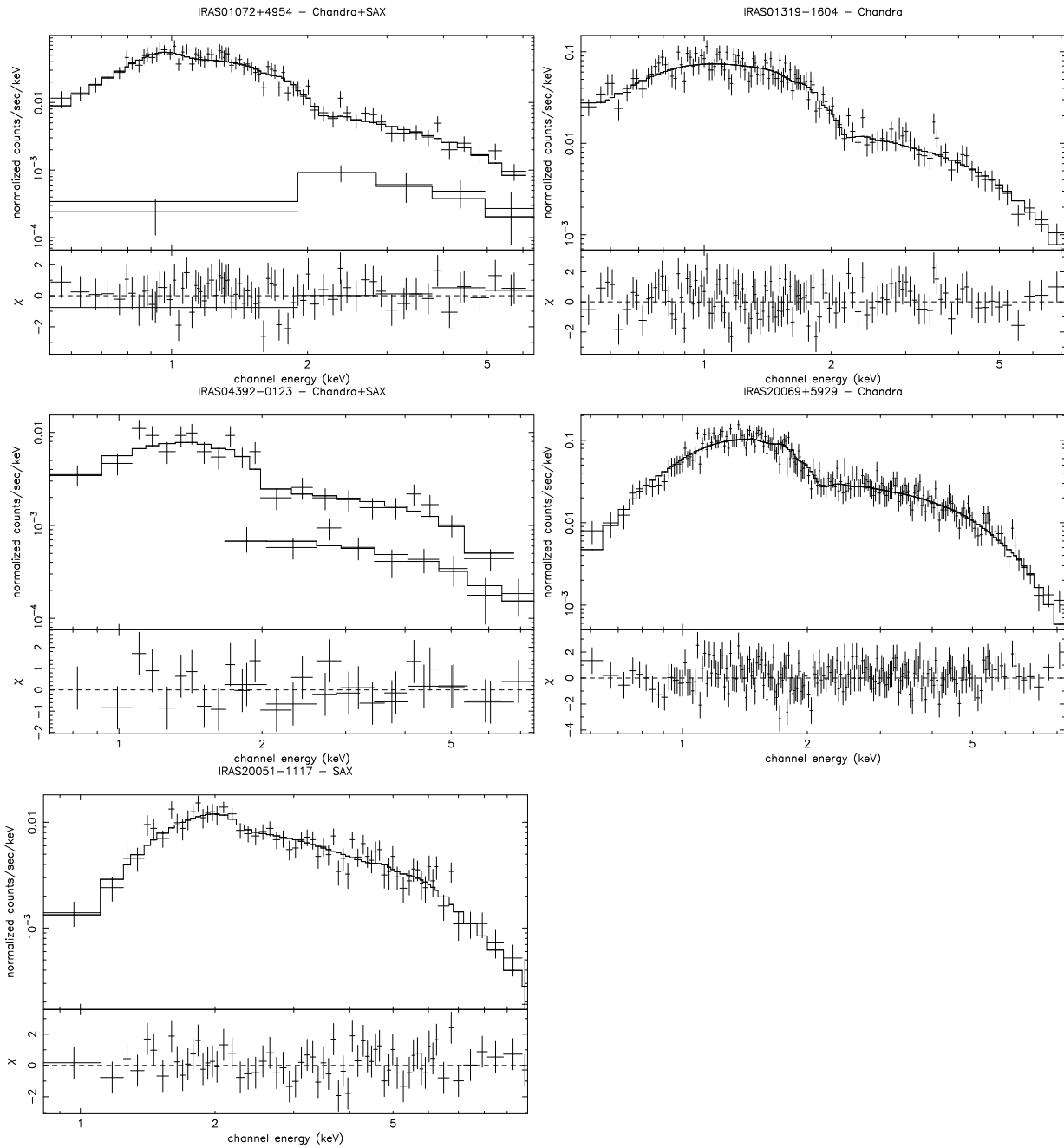


FIG. 2.— Top left: IRAS 01072+4954 - *Chandra* and *BeppoSAX* spectra fitted simultaneously with a power-law, and free relative calibration. Top right: IRAS 01319-1604 - *Chandra* spectrum modeled with a soft thermal component plus an unabsorbed power-law. Middle left: IRAS 04392-0123 - *Chandra* and *BeppoSAX* spectra fitted simultaneously with a power-law, and free relative calibration. Middle right: IRAS 20069+5929 - *Chandra* spectrum modeled with an absorbed power-law. Bottom: IRAS 20051-1117 - *BeppoSAX* spectrum modeled with a power-law and low energy absorption.

TABLE 6
Chandra AND *BeppoSAX* VARIABILITY ANALYSIS.

Name	cts/s 10^{-2}	χ^2/dof (0.3-10 keV)	cts/s 10^{-2}	χ^2/dof (0.3-2 keV)	cts/s 10^{-2}	χ^2/dof (2-10 keV)
IRAS 01072+4954	5.34±0.28	210.2/25	3.92±0.25	177.0/24	1.30±0.09	35.9/24
IRAS 01319-1604	10.20±0.37	265.3/25	7.34±0.32	208.1/25	2.77±0.21	60.1/25
IRAS 04392-0123	1.43±0.10	19.2/25	0.78±0.08	18.6/25	0.54±0.07	12.6/22
IRAS 20051-1117 ^a	3.02±0.17	29.1/18	0.85±0.09	21.7/18	2.13±0.14	32.1/18
IRAS 20069+5929	17.79±0.29	46.8/25	9.74±0.22	33.9/25	7.99±0.20	24.1/25

^a*BeppoSAX* data

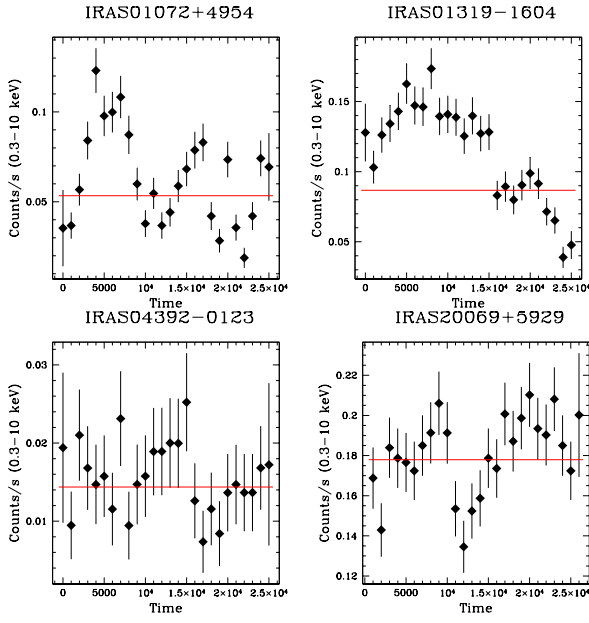


FIG. 3.— *Chandra* light curves in the 0.3-10 keV energy band binned at 1 ks (Top left: IRAS 01072+4954, Top right: IRAS 01319-1604; Bottom left: IRAS 04392-0123; Bottom right: IRAS 20069+5929).

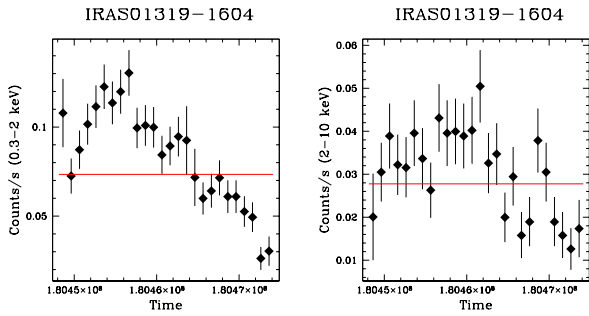


FIG. 4.— *Chandra* light curve in the soft and hard band for IRAS 01319-1604.

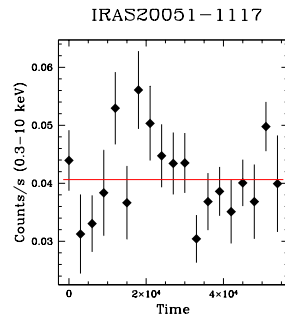


FIG. 5.— *BeppoSAX* light curve for IRAS 20051-1117 in the 0.3-10 keV energy band binned at 3 ks.

TABLE 7
LONG TERM VARIABILITY IN THE 0.3-2 KEV ENERGY BAND

Name	RASS		ROSAT PSPC		<i>BeppoSAX</i>		<i>Chandra</i>		Ratio Max/Min
	Date	Flux	Date	Flux	Date	Flux	Date	Flux	
IRAS 00317–2142	Nov 1990	5.18±0.52	Jun 1992	5.73±0.11	Nov 1995	0.79 ^a	Aug 2001	0.27 ^b	21.2
IRAS 01072+4954	Jan 1991	1.01±0.44	-	-	Jan 2002	0.32±0.06	Sept 2003	0.43±0.28	3.2
IRAS 01319–1604	Nov 1990	0.92±0.26	Jan 1992	1.98±0.17	-	-	Sept 2003	0.61±0.27	3.2
IRAS 04392–0123	Jul 1990	1.66±0.33	-	-	Nov 2001	0.09±0.009	Mar 2003	0.07±0.007	23.7
IRAS 20051–1117	Oct 1990	1.63±0.33	-	-	Oct 2001	1.88±0.10	Apr 2002	1.53 ^c	1.2
IRAS 20069+5929	Nov 1990	0.74±0.24	-	-	-	-	Mar 2003	1.33±0.03	1.8

NOTE. — Unabsorbed fluxes are in units of 10^{-12} erg cm $^{-2}$ s $^{-1}$, ratios have been calculated using the highest and the lowest flux measured.

^aASCA flux, Georgantopoulos (2000)

^bGeorgantopoulos, Zezas & Ward (2003)

^cGeorgantopoulos et al. (2004)

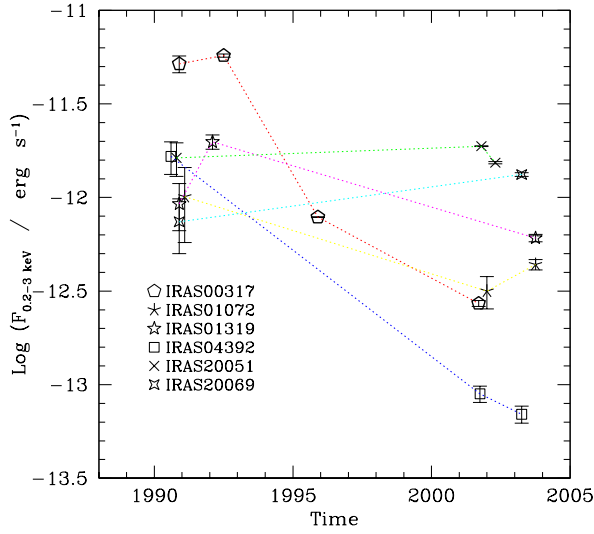


FIG. 6.— Long term trends for the 6 sources in the sample in the 0.3-2 keV band. All the fluxes reported are unabsorbed and recomputed assuming the *Chandra* spectral best-fit. Points in the 1990-1992 years are from ROSAT, in 1995 from ASCA and 2001-2003 from *BeppoSAX* and *Chandra*.

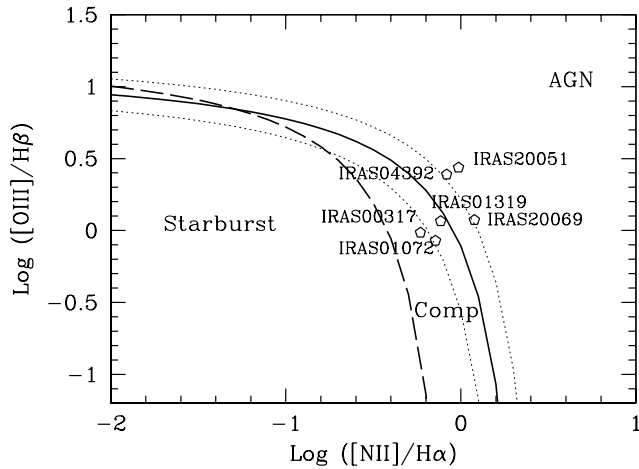


FIG. 7.— Veilleux and Osterbrock (1987) diagnostic diagrams. The optical emission line ratios are from Moran et al. (1996) and have been corrected from Galactic extinction. The solid line is the theoretical dividing line from Kewley et al. (2001) (together with the dotted lines which indicate its error range); an updated dividing (dashed) line from Kauffmann et al. (2003) has also been plotted. 'Comp' indicates the region of the diagram where Composite objects are expected to be found.

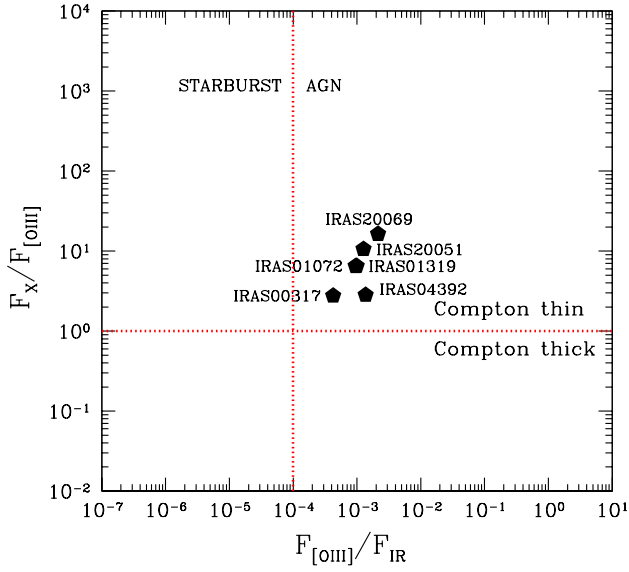


FIG. 8.— $F_X/F_{[O III]}$ vs. $F_{[O III]}/F_{IR}$. The fluxes are listed in Table 1. The $[O III]\lambda 5007$ flux of each galaxy has been corrected for the relative extinction using the formula given in Bassani et al. (1999). Compton thin, Compton thick and starburst regions (as derived in Panessa & Bassani 2002) are separated by dashed lines.

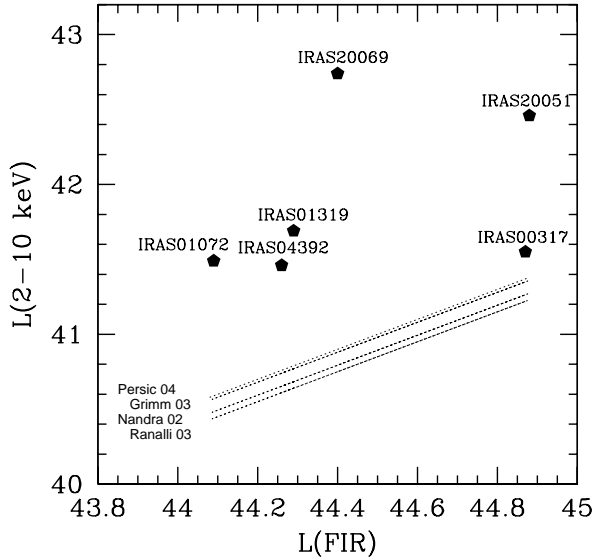


FIG. 9.— Chandra 2-10 keV luminosity vs. far-infrared luminosity for the Composites. Lines represent expected X-ray luminosity from the starbursts, following different authors, as explained in the text.

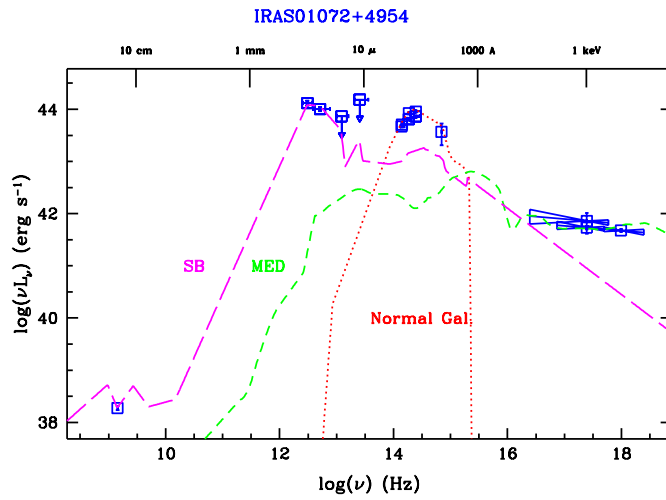
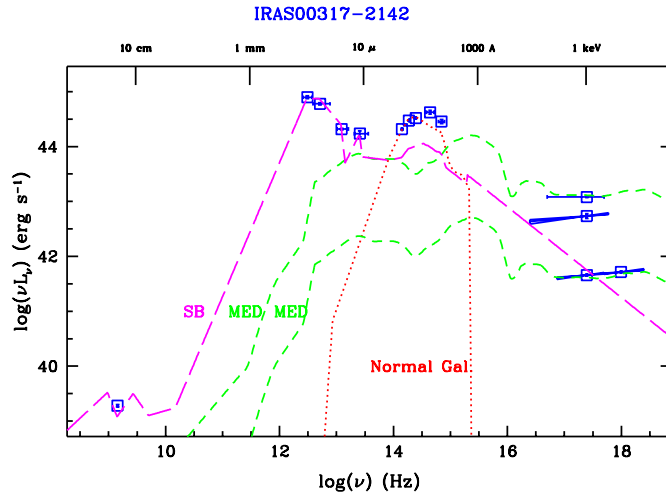
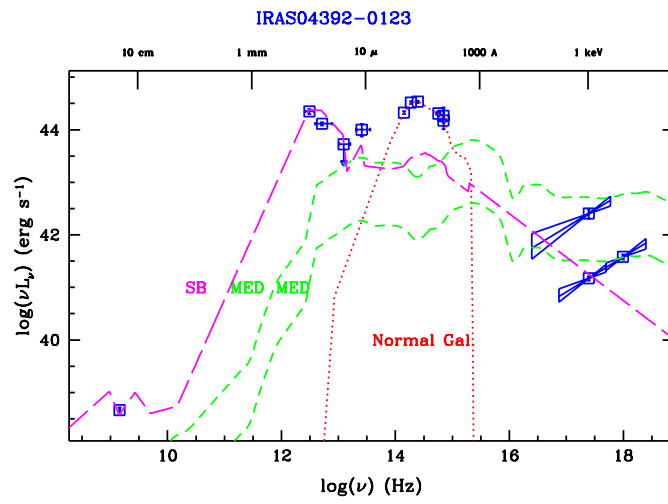
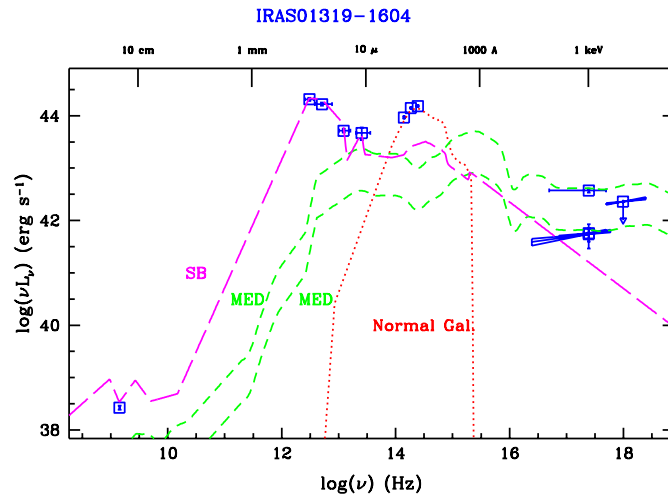
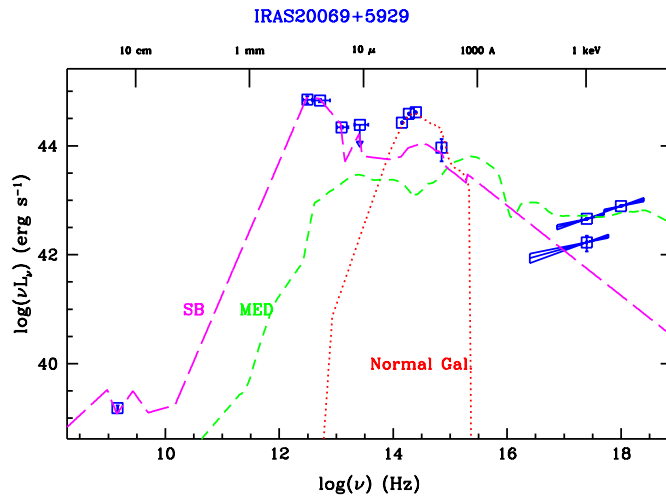
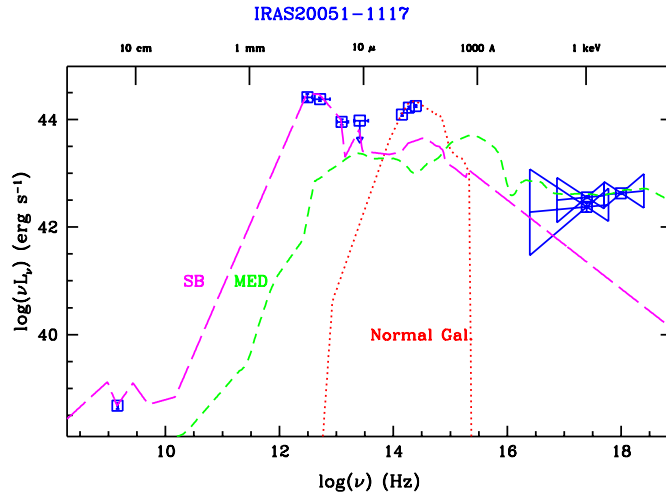


FIG. 10.— Spectral Energy Distributions for the Composite objects. Data points from the radio to the X-ray band have been plotted with their relative errors. The *Chandra* spectral slope has also been plotted. Each Composite SED have been qualitatively compared with the Medium Energy Distribution (MED) template for radio quiet quasars (short dashed lines, Elvis et al. 1994), the starburst galaxy template (long dashed lines, Schmitt et al. 1997) and the normal spiral galaxy template (dotted line, Elvis et al. 1994). In the cases of IRAS 00317–2142, IRAS 01319–1604 and IRAS 04392–0123, the MED has been plotted twice to account for the strong X-ray flux variation.

FIG. 10.— *Continue.*

FIG. 10.— *Continue.*